Characterization and Modeling of the Collision Induced Dissociation Patterns of Deprotonated Glycosphingolipids: Cleavage of the Glycosidic Bond

Marko Rožman

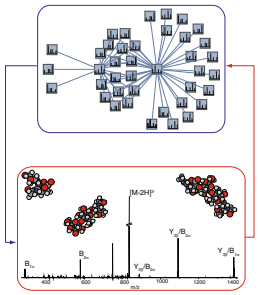

Abstract. Glycosphingolipid fragmentation behavior was investigated by combining results from analysis of a series of negative ion tandem mass spectra and molecular modeling. Fragmentation patterns extracted from 75 tandem mass spectra of mainly acidic glycosphingolipid species (gangliosides) suggest prominent cleavage of the glycosidic bonds with retention of the glycosidic oxygen atom by the species formed from the reducing end (B and Y ion formation). Dominant product ions arise from dissociation of sialic acids glycosidic bonds whereas product ions resulting from cleavage of other glycosidic bonds are less abundant. Potential energy surfaces and unimolecular reaction rates of several low-energy fragmentation pathways leading to cleavage of glycosidic bonds were estimated in order to explain observed dissociation patterns. Glycosidic bond cleavage in both neutral (unsubstituted glycosyl group) and acidic glycosphingolipids was the outcome of the charge-directed intramolecular nucleophilic substitution (S_N2) mechanism. According to the suggested mechanism, the nucleophile in a form of carboxylate or oxyanion attacks the carbon at position one of the sugar ring, simultaneously breaking the glycosidic bond and yielding an epoxide. For gangliosides, unimolecular reaction rates suggest that dominant product ions related to the cleavage of sialic acid glycosidic bonds are formed via direct dissociation channels. On the other hand, low abundant product ions related to the dissociation of other glycosidic bonds are more likely to be the result of sequential dissociation. Although results from this study mainly contribute to the understanding of glycosphingolipid fragmentation chemistry, some mechanistic findings regarding cleavage of the glycosidic bond may be applicable to other glycoconjugates.

Introduction

Characterization of glycoconjugates (glycolipids, glycosphingolipids, glycopeptides, glycosides, etc.) by tandem mass spectrometry (MS/MS) techniques has become an important part of the analytical approach to the analysis of the glycome [1–10]. In a typical scenario, glycoconjugates are ionized by electrospray ionization or matrix-assisted laser desorption ionization and subsequently analyzed by examining measured mass and collision induced dissociation (CID) spectra [1–10]. In order to optimize the application of the technique, it is important to understand the gas-phase ion chemistry of the dissociation reactions of glycoconjugates. Fast atom bombardment MS/MS investigations of glycolipids and glycopeptides have shown rather complex fragmentation patterns within the carbohydrate portion of the molecule [11–13]. Simplest fragmentation pattern results from the cleavage of the glycosidic bond, whereas the more complex processes involve the dissociation of the sugar ring, Scheme 1. Product ions on Scheme 1 are labeled according to the nomenclature proposed by Domon and Costello [12]. Product ions from the carbohydrate side are labeled as A_i, B_i, and C_i, whereas product ions containing a glycone are designated as X_j, Y_j, and Z_j. The most common dissociation pattern occurring in both positive and negative product ion spectra of glycoconjugates involves cleavage of the glycosidic bond with retention of the glycosidic oxygen atom by the species formed from the reducing end. Product ions generated via this cleavage are represented as B_i and Y_j [12].

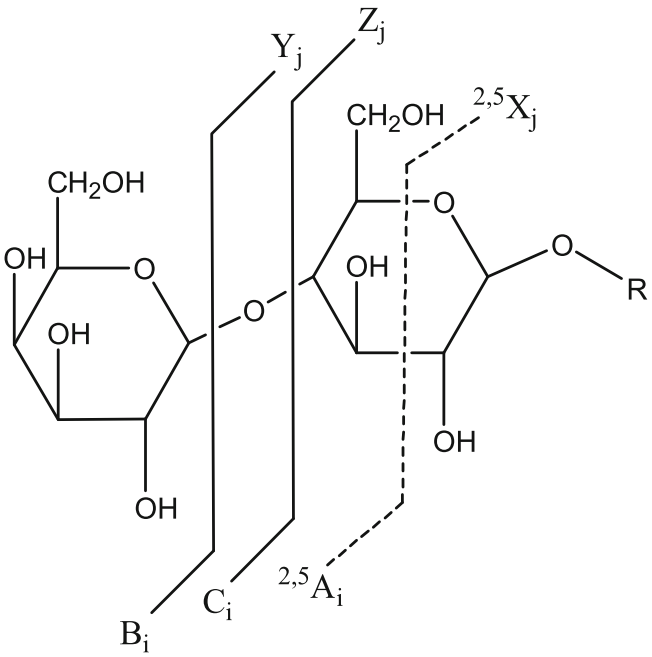

Scheme 1.

Using blocking groups and isotopic labeling experiments, Prome et al. proposed that in negative ion mode, glycosidic cleavage and formation of the Y_j ion occurs after opening the sugar ring by a vicinal attack of an oxyanion at position 4 or 6 [13]. Proton transfer reaction between the neutral and ionized fragment may occur and generate the B_i ion [12, 13]. Molecular orbital calculations at the HF/3–21G level of theory suggested that deprotonation at hydroxyl group of the non-reducing ring, accompanied by ring opening, may be an important factor in disaccharide fragmentation, especially for cross-ring cleavages [14]. On the other hand, considering data from the CID study of heparin disaccharides, Saad and Leary postulated the charge remote mechanism [15]. The general mechanism included proton transfer from hydroxylic group at position 2 to the glycosidic bond oxygen, followed by epoxide formation and cleavage of the glycosidic bond.

In our previous work we have demonstrated the computationally generated glycosphingolipid (GSL) ion database for negative ion MS and MSMS ion spectra search [16]. The database and accompanying application (GSL-finder) have been successfully applied to the analysis of mice brain gangliosides (sialic acid (Neu5Ac) containing glycosphingolipids) with altered ganglioside biosynthesis, on a commercially available ganglioside fraction, and on complex native ganglioside mixtures isolated from human (fetal and adult) and calf brain tissues [10, 16]. The GSL-finder application and other software tools for mass spectrometric data analysis of glycoconjugates are designed to assign molecular structures to tandem MS spectra [16–18]. For this strategy to be effective, fragmentation models utilized in software applications need to implement latest understandings of dissociation mechanisms of GSLs.

Having all this in mind, cleavages of the glycosidic bonds of deprotonated GSLs are examined in this study. A small data set of 75 tandem MS spectra collected from previous studies [10, 16] was used to suggest fragmentation behavior of GSLs. The proposed fragmentation pathways have been computationally assessed on a GSL level. Unraveled thermodynamics (potential energy surfaces) provided a basis for discussing kinetics aspects of the gas-phase unimolecular dissociation.

Methods

Materials, Mass Spectrometry, and Spectra Analysis

GSL tandem MS spectra were obtained from the analysis of mice, calf, and human brain tissues. Details about extraction and purification procedures can be found in the original publications [10, 16]. Negative ion mode MS and tandem MS analysis of the GSL samples were performed on the Bruker amaZon ETD ion trap system (Bruker Daltonik GmbH, Bremen, Germany) using the experimental procedure described in the previous publications [10, 16]. GSL ion identification was accomplished using the software application "GSL finder" and its accompanying GSL database [16]. Additionally, spectra were manually validated. Altogether, 75 spectra were used for analysis in this work. Computer scripts written in the Mathematica 8.0 (Wolfram Research Inc. Hanborough, United Kingdom) were used to extract and analyze tandem MS spectra.

Computational Methods

Thermodynamic and kinetic aspects of the glycosidic bond cleavage were analyzed by a combination of the quantum mechanic (QM) and the Rice-Ramsperger-Kassel-Marcus (RRKM) theory modeling. A similar approach was used for evaluating the gas-phase unimolecular dissociation of protonated peptides [19]. Potential energy surfaces of the proposed pathways were first established on the model systems (Galβ1Glc and II^3-α-Neu5Ac-Gal) and then further evaluated on GM3 (II^3-α-Neu5Ac-Galβ4Glcβ1Cer) ganglioside. In order to decrease computational resources, aliphatic chains in the ceramide were omitted.

Geometry optimizations were performed at the B3LYP/6−31G(d) level. It was suggested that using diffuse functions when dealing with negative ions should be considered [20, 21]. Effect of the diffuse function(s) on geometries and barrier heights was checked using the smaller system (Galβ4Glcβ1Cer). Comparison of geometries computed at the B3LYP/6−31G(d) level against the B3LYP/6−31+G(d) and B3LYP/6-311++G(d,p) levels did not result in any major discrepancies. Monitored reaction threshold differed up to 6 kJ mol^{-1} [B3LYP/6−31G(d) versus B3LYP/6-311++G(d,p)]. However, when using the single point calculation described below, estimated barrier heights were almost the same (S-Table 1, Supporting Information). In addition, stability of the DFT wave function was checked. In summary, considering the size of the final system (GM3 ganglioside) and the effect of the diffuse functions on calculation time, the B3LYP/6−31G(d) level of theory was used as a good compromise for

obtaining satisfactory geometries, in agreement with suggestions that it is the quickest model chemistry that delivers useful results for carbohydrates [21].

Stationary points (i.e., the minima and transition states on the potential energy surface) were identified by the harmonic frequency analysis. Transition state structures were additionally tested by the intrinsic reaction coordinate (IRC) analysis. In order to get a more accurate description of dissociation energies, single point calculations at the B3LYP/6−31G++(d,p) level were used. Energies computed at the B3LYP/6−31G++(d,p) level have shown the smallest deviation when several higher basis sets and levels of theory (e.g., MP2) were evaluated against the G3(MP2)//B3LYP (G3MP2B3) composite computational protocol [22] on a restricted number of model system molecules.

The potential energy surface of the test ganglioside (GM3) was sampled by a combination of quenched dynamics and simulated annealing. The molecular dynamics (MD) simulations at the 800 K for 30 ps were followed by slow cooling to the 200 K over 10 ps, and geometry optimization using the steepest descent approach. Five hundred structures were generated with this procedure. The structures within ~41 kJ mol^{-1} (10 kcal mol^{-1}) from the lowest energy conformer were selected as the candidate group. The candidate group structures were re-optimized using the B3LYP/6-31G(d) level of theory and energies were calculated at the B3LYP/6−31G++(d,p). The lowest energy structure found was considered as the representative structure.

All MD simulations were performed using the AMBER 99 force field, whilst quantum mechanics calculations were performed using the GAUSSIAN 09 [23]. Kinetic insights into fragmentation and rearrangement pathways were achieved by using RRKM formalism in the MassKinetics application [24]. Outputs from the QM calculations (energetic and ro-vibrational data) were used to estimate unimolecular rate constants over a range of internal energies. Geometries of all structures are available upon request.

Results and Discussion

GSL Dissociation Patterns in Tandem MS Spectra

To characterize fragmentation behavior of GSLs (mainly sialic acidic containing GSLs), 75 tandem MS spectra were analyzed (10 representative spectra can be found in Supporting Information, S-Figure 1). On average, 64% of the total ion intensity in the spectrum can be attributed to the B and Y ions. For each spectrum analyzed, B and Y product ion abundance was normalized to total abundance of all B and Y ions in the spectrum. Normalization separates the intensities of B and Y ions from other fragmentation pathways and allows direct comparison between B and Y abundances. The length of the GSL carbohydrate portion varied up to seven building blocks (three sialic acids, three hexoses, and one *N*-acetylhexosamine in a form of GT1, Supporting Information, S-Figure 1i. Forty percent spectra were from singly charged, whereas 60% spectra were from doubly charged GSLs; 45 GSLs (60%) produced B ions and 80% of them were doubly charged. When B ions are produced, they are significantly less abundant than Y ions, 20% against 80%, respectively. However, total abundance of B ions is slightly underestimated because of the use of the ion trap instrument where low mass signals (e.g., at 291*m/z* corresponding to $[Neu5Ac-H]^-$) were sometimes below the low mass cutoff range. Nevertheless, $[Neu5Ac-H]^-$ and $[Neu5Ac_2-H]^-$ represented 98% of all B ions produced. Loss of the sialic acid is also the main dissociation pattern for formation of Y ions, 73% of all Y ions correspond to $[M-Neu5Ac_n-H]^-$ type ions. Observed behavior is consistent with previous studies of N- and O-linked sialylated oligosaccharides, which found dominant fragments arising from the loss of sialic acid, and less abundant fragments from cleavage of other glycosidic bonds [2, 8]. The low-energy CID spectrum of GM3 ganglioside with (d18:1/18:0) ceramide shown in Figure 1 is an example and a brief summary of this analysis; abundant product ion(s) B_1 and Y_2 associated with the sialic acid loss are accompanied by other glycosidic bonds (Gal-Glc and Glc-Cer) dissociation product ions, Y_0 and Y_1.

Modeling of the Glycosidic Bond Cleavage of the Neutral Glycosphingolipids

Owing to the nature of extraction and purification procedures used [consult references 10, 16] only few of the neutral GSL species (species with unsubstituted glycosyl moiety) were observed (e.g., Supporting Information, S-Figure 1b). However, let us first consider possible pathways of the glycosidic bond cleavage of the neutral GSLs. One reason is that the neutral GSLs do not contain the highly acidic group (e.g., sialic acid), which strongly determinates the gas-phase chemistry, as suggested in the previous paragraph. Lack of the acidic group reduces complexity of our modeling system and we can focus on the Hex–Hex glycosidic bond cleavage that is a good example for understanding dissociation mechanisms of carbohydrates and neutral glycoconjugates. Also, the neutral GSLs are observed as product

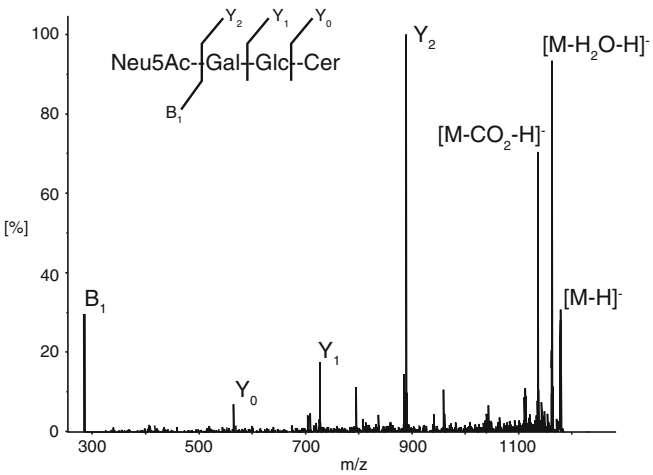

Figure 1. Product ion spectrum of the singly deprotonated ganglioside GM3 with (d18:1/18:0) ceramide

ions in tandem MS of the acidic GSL precursors (e.g., Y_0 , Y_1, and Y_2 in Figure 1) and often there is the necessity for an additional tandem MS (MS^3) experiment in order to perform thorough characterization of precursor, Figure 2.

Galβ4Glcβ1Cer (LacCer) molecule was used as model system (LacCer on Scheme 2). In the lowest energy conformation of the singly deprotonated LacCer, the charge is located on the C4 deprotonated hydroxyl group. We may presume that during vibrational excitation, proton migrates in-between hydroxylic groups, thus creating a nucleophilic center at different positions within the molecule. This presumption is supported by Salpin and Tortajada [20] suggesting that the energy barriers associated with the "proton ring walk" between hydroxylic groups of D-glucopyranose are rather small (~50 kJ mol^{-1}).

Deprotonation of the hydroxylic group may be very useful because it creates the nucleophile that can be involved in substitution reaction. In the S_N2 intramolecular nucleophilic substitution, originally suggested by Prome et al. [13], the oxyanion at position six attacks the carbon at position five and undergoes epoxide formation accompanied by opening of the sugar ring (S_N2-C5 on Scheme 2). In the second step, the glycosidic bond is cleaved to yield the Y ion. On the other hand, oxyanion at position two can attack the carbon at position one and simultaneously break the glycosidic bond and yield an epoxide (S_N2-C1 in Scheme 2). Another option is the intramolecular E2 elimination reaction, where the nucleophile removes a proton from the carbon at position two with simultaneous double bond formation and cleavage of the glycosidic bond (E2 on Scheme 2). A glycosidic bond can be also cleaved via the charge remote mechanism (proposed by Saad et al. [15]). Reaction is initiated by a proton transfer from one of the hydroxylic groups to the glycosidic bond oxygen, followed by an epoxide formation and cleavage of the glycosidic bond (CR–PT in Scheme 2). Note that the charge remote mechanism mainly produces B ions.

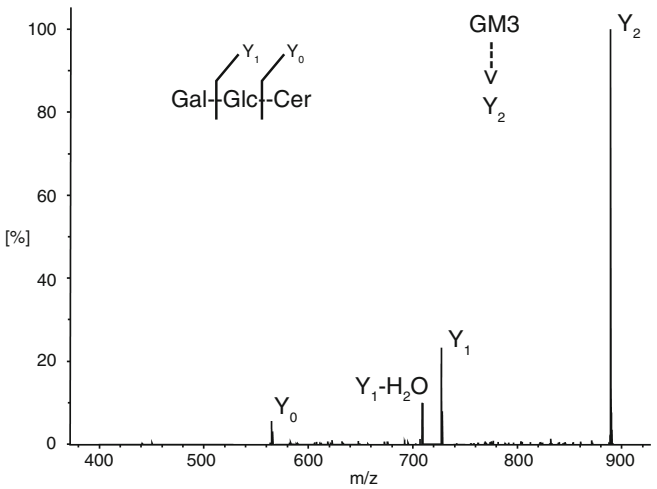

Figure 2. Collision induced dissociation MS^3 product ion spectrum of Y_2 (Galβ4Glcβ1Cer). Y_2 product ion derives from the fragmentation of GM3 ganglioside with (d18:1/18:0) ceramide (MS^2 spectrum depicted in the Figure 1)

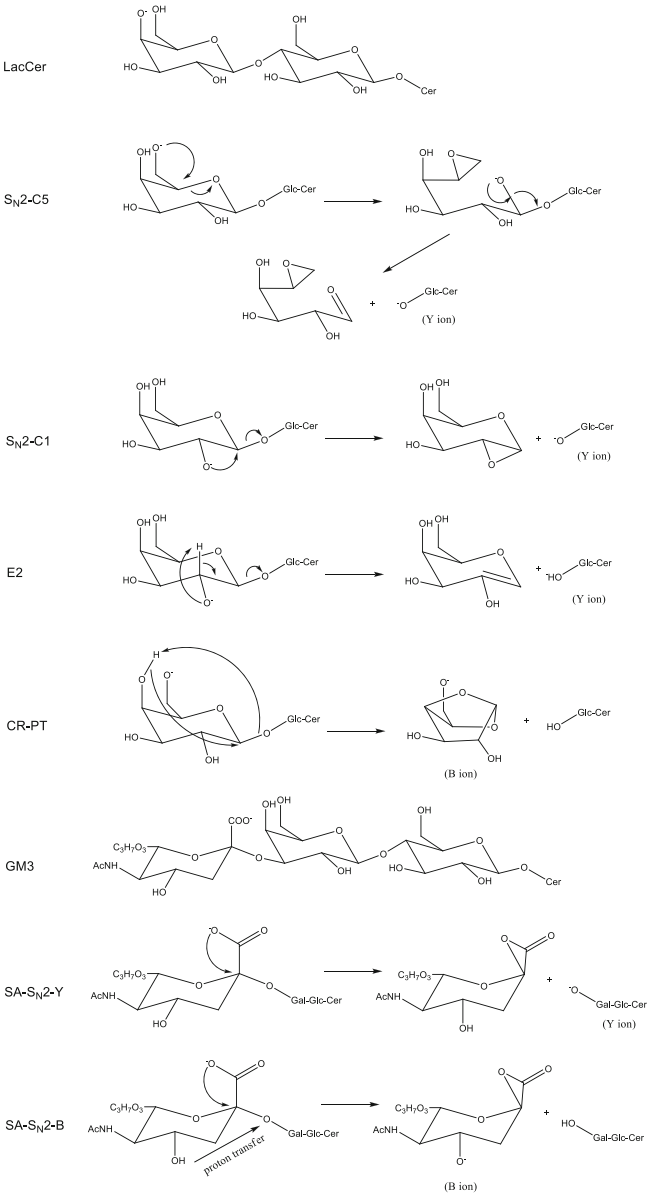

Scheme 2.

Calculated reaction barriers indicate that the lowest energy pathways are associated with S_N2 mechanisms (Table 1). The S_N2-C5 mechanism on the Glc ring has a higher energy barrier than the rest of the S_N2 pathways. This is probably due to specific configuration of the transition state with the oxyanion at the reaction center lacking the hydrogen bonding (Supporting Information, S-Figure 2e). RRKM reaction rates show that at the ms and μs time scale the S_N2 mechanism is dominant (Figure 3). At the μs time range there could be some minor E2 elimination product ions. Gal–Glc glycosidic bond cleavage mainly proceeds via both S_N2 pathways (C1 and C5), whereas Glc–Cer glycosidic bond cleavage just via S_N2-C1. Two pathways contribute to the formation of Y_1 ion, whereas only one to Y_0 in agreement with observation that Y_0 ion is less abundant than Y_1 (Figure 2). Overall, both S_N2 mechanisms are consistent with isotopic labeling experiments [13] and

Table 1. B3LYP/6-31++G(d,p)//B3LYP/6-31G(d) Energies (in *E*h) and Relative Energies (in kJ mol^{-1}) of Conformers for Glycosidic Bond(s) Cleavage of LacCer. The Relative Energies Were Calculated with Respect to the Most Stable LacCer Conformer Found. Transition State Structures can be Found in Supporting Information (S-Figure 2)

Bond	Reaction type	Intermediate	*E*	Δ
Gal-Glc	S_N2–C5	R	–1738.003074	9.9
		TS	–1737.958758	126.2
		P	–1737.976295	80.2
		TS2	–1737.956259	132.8
		P2	–1737.973096	88.6
Gal–Glc	S_N2–C1	R	–1737.97317	88.4
		TS	–1737.956999	130.8
		P	–1737.996769	26.4
Gal–Glc	E2	R	–1737.98145	66.6
		TS	–1737.938313	179.9
		P	–1738.013044	–16.3
Gal–Glc	Charge remote	R	–1737.985802	55.2
		TS	–1737.897208	287.8
		P	–1737.948628	152.8
Glc-Cer	S_N2–C5	R	–1737.965260	109.2
		TS	–1737.937260	182.7
		P	–1737.954909	136.3
		TS2	–1737.949812	149.7
		P2	–1737.951950	144.1
Glc–Cer	S_N2–C1	R	–1737.983760	60.6
		TS	–1737.951631	144.9
		P	–1737.974633	84.5
Glc-Cer	E2	R	–1737.988918	47.0
		TS	–1737.924703	215.6
		P	–1737.964200	111.9
Glc-Cer	Charge remote	R	–1737.979529	71.7
		TS	–1737.901013	277.8
		P	–1737.959541	124.2

theoretical calculations [14] that found oxyanion formation at the non-reducing ring to be an important factor in the glycosidic bond cleavage process. In this case, our results suggest slight preference of the one-step mechanism of the glycosidic bond cleavage (S_N2-C1 in Scheme 2) over the previously proposed two-step process [12, 13], which involves sugar ring opening (S_N2-C5 on Scheme 2). However, as already suggested, this is due to particular transition state conformation, and with other glycoconjugate structure probably both pathways are operating. Moreover, first step of the S_N2-C5 mechanism produces an important intermediate, which is most likely a branching point between the glycosidic bond cleavage and more complex pathways involving cleavage(s) of the carbon–carbon bond(s) and sugar ring fragmentation(s).

Now that we explored mechanisms of the glycosidic bond cleavage on a simple Hex–Hex system, we can add the acidic group (i.e., Neu5Ac) to our system. Sialic acid group represents a new charge center that will strongly influence the gas-phase chemistry of (from now) acidic GSL (i.e., gangliosides).

Modeling of the Glycosidic Bond Cleavage of Deprotonated Gangliosides

To explain dissociation patterns of deprotonated gangliosides and to suggest appropriate fragmentation paths, GM3 ganglioside was used (GM3 on Scheme 2). In the lowest energy conformation of the $[GM3\text{-}H]^-$ ion, carboxylic group of Neu5Ac is deprotonated. Deprotonation of the carboxylic group creates the nucleophile, which can initiate substitution reaction. In the S_N2 intramolecular nucleophilic substitution, the carboxylic group attacks the Neu5Ac aliphatic carbon at position one, causing cleavage of the glycosidic bond and formation of the Y_2 ion (S_N2-SA-Y in Scheme 2). This process may be accompanied by proton shifting [from the C(4) hydroxyl group to the glycosidic bond oxygen] in the transition state to yield the B_1 ion (S_N2-SA-B on Scheme 2). Barriers associated with formation of the B_1 and Y_2 ion via S_N2-SA pathways are 128 and 172 kJ mol^{-1}, respectively (Table 2). E2 elimination and charge remote mechanism were not considered for loss of the sialic acid because of difficulties with locating corresponding transition state (E2 – problem with stabilizing protonated carboxylic group at close proximity of the reaction center, CR-PT – problem with epoxide formation on the C1 atom without involvement of the carboxylic group).

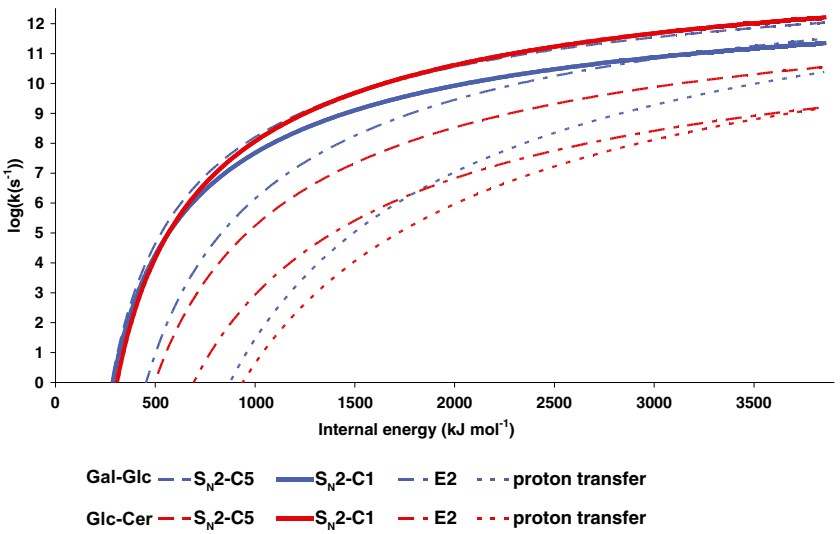

Figure 3. RRKM theory unimolecular reactions rate constants for dissociation of glycosidic bonds in LacCer

Table 2. B3LYP/6-31++G(d,p)//B3LYP/6-31G(d) Energies (in *E*h) and Relative Energies (in kJ mol^{-1}) of Conformers for Glycosidic Bond(s) Cleavage of GM3 Ganglioside. The Relative Energies Were Calculated with Respect to the Most Stable GM3 Conformer Found. Transition State Structures can be Found in Supporting Information (S-Figure 3)

Bond	Reaction type	Intermediate	*E*	Δ
Neu5Ac–Gal	S_N2-SA-B	R	–2824.075753	9.1
		TS	–2824.030438	128.0
		P	–2824.032387	122.9
Neu5Ac–Gal	S_N2-SA-Y	R	–2824.076812	6.3
		TS	–2824.013697	172.0
		P	–2824.014888	168.9
Gal–Glc	S_N2–C5	R	–2824.079203	0.0
		TS	–2823.995897	218.7
		P	–2824.009896	182.0
		TS2	–2823.989041	236.7
		P2	–2823.990992	231.6
Gal–Glc	S_N2–C1	R	–2824.061720	45.9
		TS	–2823.988306	238.6
		P	–2824.031523	125.2
Gal–Glc	E2	R	–2824.042775	95.6
		TS	–2823.978987	263.1
		P	–2824.034291	117.9
Gal–Glc	Charge remote	R	–2824.061720	45.9
		TS	–2823.996924	216.0
		P	–2824.048505	80.6
Glc–Cer	S_N2–C5	R	–2824.073657	14.6
		TS	–2823.978880	263.4
		P	–2823.988706	237.6
		TS2	–2823.988425	238.3
		P2	–2823.988885	237.1
Glc–Cer	S_N2–C1	R	–2824.069352	25.9
		TS	–2823.984889	247.6
		P	–2824.001977	202.8
Glc–Cer	E2	R	–2824.001073	205.1
		TS	–2823.938737	368.8
		P	–2824.001277	204.6
Glc–Cer	Charge remote	R	–2824.055108	63.3
		TS	–2823.986391	243.7
		P	–2824.025755	140.3

Dissociation of both Gal–Glc and Glc–Cer glycosidic bonds of GM3 ganglioside (i.e., yield of the Y_0 and Y_1 ions, Figure 1) may be rationalized via already assessed charge directed and charge remote mechanisms (Scheme 2). However, for the charge directed mechanisms, deprotonated hydroxyl group is needed. In order to create deprotonated hydroxyl, proton transfer between deprotonated carboxyl group and the hydroxyl must occur. Considering the strong difference in the gas-phase acidities between these two functional groups, two scenarios were tested. In the first, multistep pathway, proton transfer between deprotonated carboxyl group and the hydroxyl is followed by conformational rearrangement and glycosidic bond dissociation (Supporting Information, S-Scheme 1a). The second scenario represents a concerted mechanism, which includes glycosidic bond cleavage accompanied with a proton walk from the active hydroxyl to deprotonated carboxyl group (Supporting Information, S-Scheme 1b).

According to the first scenario, formation of the deprotonated hydroxylic group (Gal C4) requires 188.8 kJ mol^{-1}. Deprotonation is followed by a proton ring walk and conformational rearrangement (not assessed) in order to form intermediates for [e.g., the S_N2 reaction (on Gal C1) with dissociation thresholds of 244 kJ mol^{-1}]. On the other hand, concerted mechanism is much simpler and reactants are either the most stable GM3 conformation or conformers slightly higher in energy (stabilized with multiple hydrogen bonds, perfectly aligned for proton walk). Reaction barrier of the concerted S_N2 pathway (in Gal C1) is 238.6 kJ mol^{-1}. Taking into account that concerted pathways have straightforward reaction path (one high threshold instead of multiple) and slightly lower thresholds, in further evaluation of the charge directed mechanisms we opted for concerted pathways.

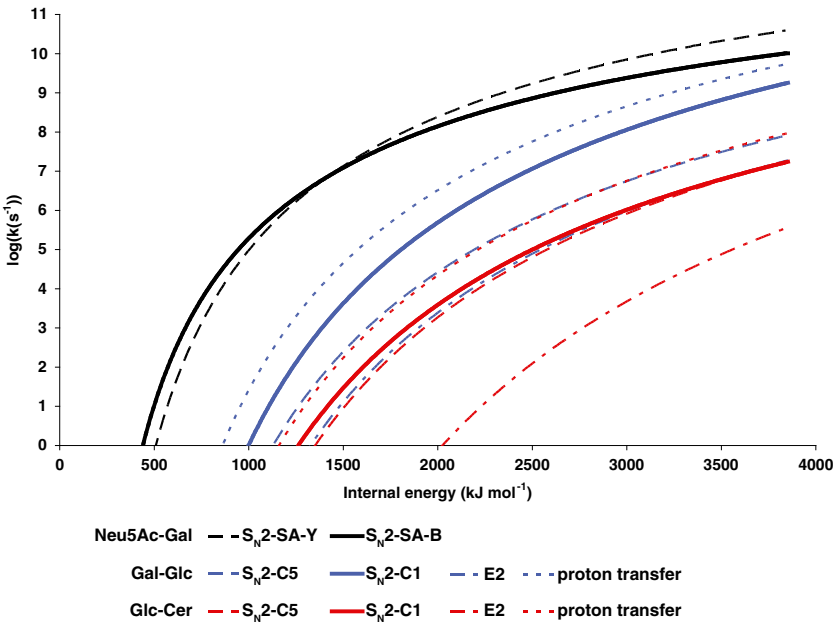

Figure 4. RRKM theory unimolecular reactions rate constants for dissociation of glycosidic bonds in GM3 (II^3-α-Neu5Acβ4Glcβ1Cer) ganglioside

Summarizing all evaluated pathways, we can notice that lowest barrier is associated with the cleavage of Neu5Ac–Gal glycosidic bond via the charge directed SA-S_N2-(B or Y) mechanism (Table 2). Charge remote and S_2N charge directed mechanisms are the lowest energy pathways for the Gal–Glc and Glc–Cer glycosidic bonds cleavage. However, Hex–Hex bond cleavage is ~90 kJ mol^{-1} higher than Neu5Ac–Hex bond cleavage, suggesting that a majority (in some cases perhaps all) of the product ions would be associated with the Neu5Ac–Gal glycosidic bond cleavage.

Calculated unimolecular reaction rates (by the RRKM theory) show that for reaching both ms and μs time range, the charge directed SA-S_N2-(B or Y) pathway (cleavage of the Neu5Ac–Gal glycosidic bond) requires least energy (665 and 1165 kJ mol^{-1}, respectively), Figure 4. Considerably more energy is required for cleavage of the Gal–Glc (1200 to 1835 kJ mol^{-1}, respectively) and the Glc–Cer (1640 to 2605 kJ mol^{-1}, respectively) glycosidic bonds in the ms and μs time range. In the context of tandem MS ion abundances, obtained results suggest that in the GM3 product ion spectrum, product ions related to loss of the sialic acid (B_1 and Y_2) would be dominant. One can notice that addition of the sialic acid to the neutral glycoconjugate chain strongly influences the gas-phase chemistry, focusing reactivity towards acidic group. This is in agreement with the obtained product ion spectrum of GM3 (d18:1/18:0) depicted in Figure 1, as well as with analysis of gangliosides fragmentation behavior (vide supra). For the Neu5Ac–Gal glycosidic bond cleavage, modeling results (Figure 4) imply that B_1 product ion should be slightly more abundant over Y_2 ion. Although this is not in total agreement with the experimental data (Figure 1), it is possible that relative abundances of B versus Y ions associated with the Neu5Ac–Gal glycosidic bond cleavage can vary as a consequence of glycoconjugate secondary structure and relative position of hydroxylic groups in the vicinity of the reaction center. Also, the proton transfer in an ion-neutral post-dissociation complex can occur causing the Y ion domination.

According to the RRKM calculations, the fastest Hex–Hex bond cleavage occurs at the sub-millisecond time scale roughly at the same internal energy when the charge directed SA-S_N2 pathway reaches the microsecond time frame, implying very low abundance of Hex–Hex bond cleavage product ions. Mechanism associated with fastest Hex–Hex bond cleavage is the charge remote mechanism and it should result in B ion series (e.g., B_2 and B_3). However, B ions arising from the Gal–Glc and Glc–Cer glycosidic bond cleavages are not observed in GM3 product ion spectrum (Figure 1). Moreover, our data on GSLs dissociation patterns in the ion trap tandem MS show their minor intensities (vide supra). Overall data suggest either the existence of some other Hex–Hex bond dissociation pathway (not considered here) or, more likely, a sequential dissociation of Y_2 product ion and formation of Y_1 and Y_0. The MS^3 product ion spectrum of Y_2 supports the fact that Y_2 ion can produce Y_1 and Y_0 product ions in a possible sequential dissociation event (Figure 2).

Conclusion

The cleavage of the glycosidic bond with retention of the glycosidic oxygen atom by the species formed from the reducing end of GSL has been studied experimentally and computationally. Important findings can be summarised as follows: The analysis of 75 tandem MS spectra of mainly acidic GSLs (gangliosides) show that the dominant dissociation pattern is the cleavage of the sialic acid glycosidic bonds with formation of both B and Y product ions. Cleavages of other glycosidic bonds are less abundant and mostly Y product ions are observed.

Molecular modeling work on the neutral GSL suggests that observed cleavages of glycosidic bonds are a combination of two charge-directed intramolecular nucleophilic substitution (S_N2) mechanisms: (1) one-step process that simultaneously breaks the glycosidic bond and yields an epoxide, and (2) two-step process that includes epoxide formation and sugar ring opening followed by cleavage of the glycosidic bond. The RRKM results somewhat favor the one-step mechanism.

For the acidic GSLs, molecular modeling indicates that the major pathway is loss of the sialic acid via S_N2 mechanism. The reaction occurs when the nucleophile in a form of carboxylate attacks the carbon at position one of the sugar ring and simultaneously breaks the glycosidic bond to yield an epoxide. Unimolecular reaction rates show that product ions related to the cleavage of sialic acid glycosidic bond are dominant. For cleavage of other glycosidic bonds, overall data suggest activation of sequential dissociation channels.

More generally, this work provides insights into the glycosidic bond dissociation pathways that may be of particular value to other glycoconjugate studies.

Acknowledgment

Helpful discussions with Laboratory members are gratefully acknowledged. The Ministry of Science, Education, and Sports of Republic of Croatia supported this work (Grant Number: 098-0982915-2945).

References

1. Chai, W., Piskarev, V., Lawson, A.M.: Branching pattern and sequence analysis of underivatized oligosaccharides by combined MS/MS of singly and doubly charged molecular ions in negative-ion electrospray mass spectrometry. J. Am. Soc. Mass Spectrom. **13**, 670–679 (2002)
2. Karlsson, N.G., Wilson, N.L., Wirth, H.J., Dawes, P., Joshi, H., Packer, N.H.: Negative ion graphitised carbon nano-liquid chromatography/mass spectrometry increases sensitivity for glycoprotein oligosaccharide analysis. Rapid Commun. Mass Spectrom. **18**, 2282–2292 (2004)
3. Yang, K., Cheng, H., Gross, R.W., Han, X.: Automated lipid identification and quantification by multidimensional mass spectrometry-based shotgun lipidomics. Anal. Chem. **81**, 435–4368 (2009)
4. Wenk, M.R.: Lipidomics: new tools and applications. Cell **143**, 888–895 (2010)
5. Wada, Y., Dell, A., Haslam, S.M., Tissot, B., Canis, K., Azadi, P., Bäckström, M., Costello, C.E., Hansson, G.C., Hiki, Y., Ishihara, M., Ito, H., Kakehi, K., Karlsson, N., Hayes, C.E., Kato, K., Kawasaki, N., Khoo, K.-H., Kobayashi, K., Kolarich, D., Kondo, A., Lebrilla, C., Nakano, M., Narimatsu, H., Novak, J., Novotny, M.V., Ohno, E., Packer, N.H., Palaima,

E., Renfrow, M.B., Tajiri, M., Thomsson, K.A., Yagi, H., Yu, S.-Y., Taniguchi, N.: Comparison of methods for profiling O-glycosylation. Mol. Cell. Proteomics **9**, 719–727 (2010)
6. Műthing, J., Distler, U.: Advances on the compositional analysis of glycosphingolipids combining thin-layer chromatography with mass spectrometry. Mass Spectrom. Rev. **29**, 425–479 (2010)
7. Sullards, M.C., Liu, Y., Chen, Y., Merrill, J.: Analysis of mammalian sphingolipids by liquid chromatography tandem mass spectrometry (LC-MS/MS) and tissue imaging mass spectrometry (TIMS). Biochim. Biophys. Acta Mol. Cell Biol. Lipids **1811**, 838–853 (2011)
8. Doohan, R.A., Hayes, C.A., Harhen, B., Karlsson, N.G.: Negative ion CID fragmentation of O-linked oligosaccharide aldoses—charge induced and charge remote fragmentation. J. Am. Soc. Mass Spectrom. **22**, 1052–1062 (2011)
9. Zamfir, A., Serb, A., Vukelić, Ž., Flangea, C., Schiopu, C., Fabris, D., Kalanj-Bognar, S., Capitan, F., Sisu, E.: Assessment of the molecular expression and structure of gangliosides in brain metastasis of lung adenocarcinoma by an advanced approach based on fully automated chip-nanoelectrospray mass spectrometry. J. Am. Soc. Mass Spectrom. **22**, 2145–2159 (2011)
10. Mlinac, K., Fabris, D., Vukelić, Ž., Rožman, M., Heffer, M., Kalanj Bognar, S.: Structural analysis of brain ganglioside acetylation patterns in mice with altered ganglioside biosynthesis. Carbohydr. Res. **382**, 1–8 (2013)
11. Barber, M., Bordoli, R.S., Sedgwick, R.D., Vickerman, J.C.: Fast atom bombardment mass spectrometry (FAB) negative-ion spectra of some simple monosaccharides. J. Chem. Soc. Faraday Trans. 1 **78**, 1291–1296 (1982)
12. Domon, B., Costello, C.E.: A systematic nomenclature for carbohydrate fragmentations in FAB-MS MS spectra of glycoconjugates. Glycoconj. J. **5**, 397–409 (1988)
13. Prome, J.-C., Aurelle, H., Prome, D., Savagnac, A.: Gas phase glycosidic cleavage of oxynions from alkyl glycosides. Org. Mass Spectrom. **22**, 6–12 (1987)
14. Mulroney, B., Peel, J.B., Traeger, J.C.: Theoretical study of deprotonated glucopyranosyl disaccharide fragmentation. J. Mass Spectrom. **34**, 856–871 (1999)
15. Saad, O.M., Leary, J.A.: Delineating mechanisms of dissociation for isomeric heparin disaccharides using isotope labeling and ion trap tandem mass spectrometry. J. Am. Soc. Mass Spectrom. **15**, 1274–1286 (2004)
16. Rožman, M., Fabris, D., Mrla, T., Vukelić, Ž.: Database and data analysis application for structural characterization of gangliosides and sulfated glycosphingolipids by negative ion mass spectrometry. Carbohydr. Res. **400**, 1–8 (2014)
17. Fahy, E., Sud, M., Cotter, D., Subramaniam, S.: LIPID MAPS online tools for lipid research. Nucleic Acids Res. **35**, W606–W612 (2007)
18. Souady, J., Dadimov, D., Kirsch, S., Bindila, L., Peter-Katalinić, J., Vakhrushev, S.Y.: Software utilities for the interpretation of mass spectrometric data of glycoconjugates: application to glycosphingolipids of human serum. Rapid Commun. Mass Spectrom. **24**, 1039–1048 (2010)
19. Rožman, M.: Modelling of the gas-phase phosphate group loss and rearrangement in phosphorylated peptides. J. Mass Spectrom. **46**, 949–955 (2011)
20. Salpin, J.-Y., Tortajada, J.: Gas-phase acidity of D-glucose. A density functional theory study. J. Mass Spectrom. **39**, 930–941 (2004)
21. Csonka, G.I., French, A.D., Johnson, G.P., Stortz, C.A.: Evaluation of density functionals and basis sets for carbohydrates. J. Chem. Theory Comput. **5**, 679–692 (2009)
22. Baboul, A.G., Curtiss, L.A., Redfern, P.C., Raghavachari, K.: Gaussian-3 theory using density functional geometries and zero-point energies. J. Chem. Phys. **110**, 7650–7657 (1999)
23. Frisch, M.J., Trucks, G.W., Schlegel, H.B., Scuseria, G.E., Robb, M.A., Cheeseman, J.R., Scalmani, G., Barone, V., Mennucci, B., Petersson, G.A., Nakatsuji, H., Caricato, M., Li, X., Hratchian, H.P., Izmaylov, A.F., Bloino, J., Zheng, G., Sonnenberg, J.L., Hada, M., Ehara, M., Toyota, K., Fukuda, R., Hasegawa, J., Ishida, M., Nakajima, T., Honda, Y., Kitao, O., Nakai, H., Vreven, T., Montgomery Jr., J.A., Peralta, J.E., Ogliaro, F., Bearpark, M., Heyd, J.J., Brothers, E., Kudin, K.N., Staroverov, V.N., Keith, T., Kobayashi, R., Normand, J., Raghavachari, K., Rendell, A., Burant, J.C., Iyengar, S.S., Tomasi, J., Cossi, M., Rega, N., Millam, J.M., Klene, M., Knox, J.E., Cross, J.B., Bakken, V., Adamo, C., Jaramillo, J., Gomperts, R., Stratmann, R.E., Yazyev, O., Austin, A.J., Cammi, R., Pomelli, C., Ochterski, J.W., Martin, R.L., Morokuma, K., Zakrzewski, V.G., Voth, G.A., Salvador, P., Dannenberg, J.J., Dapprich, S., Daniels, A.D., Farkas, O., Foresman, J.B., Ortiz, J.V., Cioslowski, J., Fox, D.J.: Gaussian 09. Gaussian Inc, Wallingford (2013)
24. Drahos, L., Vékey, K.: MassKinetics: a theoretical model of mass spectra incorporating physical processes, reaction kinetics, and mathematical descriptions. J. Mass Spectrom. **36**, 237–263 (2001)